Atmospheric Research, Manuscript No. _____

Lightning evolution related to radar–derived microphysics in the 21 July 1998 EULINOX supercell storm

Nikolai Dotzek [1], Hartmut Höller [1], Claire Théry [2], and Thorsten Fehr [1]

[1] DLR–Institut für Physik der Atmosphäre,
Oberpfaffenhofen, D–82234 Wessling, Germany

[2] ONERA–DMPH,
BP 72–29, F–92322 Châtillon Cedex, France

Special Issue: Proc. 1st Conf. on European Tornadoes and Severe Storms

Received 10 May 2000, in revised form

Corresponding author's address:
Dr. N. Dotzek
DLR–Institut für Physik der Atmosphäre,
Oberpfaffenhofen, D–82234 Wessling, Germany.
E–mail: nikolai.dotzek@dlr.de,
Tel: +49–8153–28–1845, Fax: +49–8153–28–1841.

Submitted to *Atmos. Res.*

Lightning evolution related to radar–derived microphysics in the 21 July 1998 EULINOX supercell storm

Nikolai Dotzek [1], Hartmut Höller [1], Claire Théry [2], and Thorsten Fehr [1]

[1] DLR–Institut für Physik der Atmosphäre,
Oberpfaffenhofen, D–82234 Wessling, Germany

[2] ONERA–DMPH,
BP 72–29, F–92322 Châtillon Cedex, France

Received 10 May 2000, in revised form

Abstract

Results of a combined analysis of data from a C–band polarimetric Doppler radar and a 3D VHF interferometric lightning mapping system as obtained during the EULINOX field campaign are presented. For 21 July 1998 the lightning data from a supercell thunderstorm weakly indicate a tendency for a bi–level vertical distribution of lightning VHF emissions around the –15° C and –30° C temperature levels. Also, in some parts of the clouds, evidence is found for the presence of a lower positive charge center near the freezing level. However, where strong vertical motions prevail VHF emissions are not organized in horizontal layers but in oblique or vertical regions. Correlation of VHF signals with radar quantities shows that in the growing storm peak VHF activity is low and related to reflectivity factors around 30 dBZ, while after the mature stage the peak VHF activity is about three times larger. The highest density of VHF signals is now found near reflectivity factors of 45 dBZ. A polarimetric hydrometeor classification indicates that during storm development most lightning activity occurs where graupel and, secondarily, snow and small dry hail are present. In the decaying phase of the supercell hailstorm, however, most lightning VHF emissions stem from the region with hail and heavy rain. Furthermore, while the VHF signal frequency per km^3 in the graupel and rain regions remains nearly constant throughout the supercell life cycle, the signal frequency in the hail region rises during storm decay.

Keywords: Lightning; EULINOX, Supercell storm

1 Introduction

The 1998–1999 **Eu**ropean **Li**ghtning **N**itrogen **Ox**ides project (EULINOX) aimed at an improved understanding of the processes of lightning–induced NO_X production within central European thunderstorms (Höller et al., 1999b, 2000). Similar to the earlier LINOX campaign (Huntrieser et al., 1998; Höller et al., 1999a) the main objective was to obtain a more reliable estimation of this natural NO_X source (Dotzek et al., 2000a; Théry et al., 2000) compared to man–made and other natural sources, such as fuel combustion in ground and air traffic, industry or in–soil nitrogen fixation by bacteria (cf. Lee et al., 1997).

During the summer 1998 EULINOX intensive observation period in southern Germany (cf. the map in Fig. 1) a great variety of analysis methods was applied. Aside from aircraft measurements of chemical constituents within and around thunderclouds, C–band Doppler radars, mesonet stations and radiosondes contributed to the EULINOX data base. Also, interferometric measurements of VHF sources from lightning discharges in two and three dimensions were made by the ONERA, complementary to those of a two–dimensional LPATS (Lightning Positioning and Tracking System) network (Théry, 2000).

The ONERA interferometric lightning mapper (ITF) consisted of two VHF interferometric antenna stations ($\diamond$ in Fig. 1) 40 km apart, at 25 km on the ENE and SSW sides of the operational center at DLR in Oberpfaffenhofen ($+$ in Fig. 1). Certain parts of intracloud or cloud–to–ground lightning flashes emit strongly in the VHF band. The two interferometric stations detect this radiation in a narrow band (1 MHz width) at 114 MHz and record its amplitude and direction of arrival with a 23 μs sampling interval. The ITF mapping system can detect negative leaders and high current discharges (intracloud recoil streamers, cloud–to–ground dart leaders and return strokes) all along their propagation paths (Defer, 1999). Both stations give the azimuth of the VHF sources, and in addition the southern station can also measure the source elevation. The x,y–position of a source is determined from the azimuthal directions relative to the two stations, while the elevation allows for retrieval of the source altitude. Single VHF signals are then grouped in "bursts", corresponding to individual discharges. Flashes are identified as a succession of such bursts. Note that the accuracy of the elevation sensor decreases rapidly for very low (below 5°) and very high (above 48°) elevations. Therefore, a storm can be coherently observed from 2 km AGL up to 11 km only if it is within 10 km and 25 km distance from the southern interferometric station. These range rings are indicated by circles in Fig. 1.

Furthermore, the C–band polarimetric Doppler radar POLDIRAD at DLR in Oberpfaffenhofen provided three–dimensional information on the storm's dynamical and microphysical structure, allowing for an identification of the different hydrometeor types in the thundercloud and the accompanying anvil region. Therefore the combination of data from ONERA's VHF interferometric lightning mapper and DLR's polarization diversity radar was expected to provide a detailed view of the evolution of the lightning activity (defined as number of VHF sources per unit space and time) and its relation to cloud microphysics and dynamics.

The purpose of this paper is to shed light on the cloud microphysical processes which enable or enhance the charge separation mechanisms inside a cumulonimbus cloud. The main objectives of this twofold radar–VHF interferometer approach to the cloud electrification problem were:

- identification of the main regions or levels of lightning activity inside the cloud and comparison to theoretical predictions,
- quantification of the vertical extent of single flashes, and clarification of how lightning activity was distributed inside the cloud,
- identification of correlations between lightning discharges and certain hydrometeor types or radar parameters, such as the reflectivity factor.

The paper is organized as follows: Sec. 2 briefly reviews the life–cycle of the supercell hailstorm before in Sec. 3 the vertical distribution of VHF activity due to lightning flashes is described. The relation between lightning VHF sources and cloud microphysics is treated in Sec. 4, while Secs. 5 and 6 present a discussion of results and conclusions.

2 Life cycle of the supercell storm

The data evaluation is focused on a supercell storm of 21 July 1998 (Höller et al., 1999b, 2000). On this day thunderstorms approached the Munich region from the west, leading to widespread deep convective cells over southern Germany and eastern neighboring countries during the afternoon and evening. Some of the storms became severe: aside from some hail swaths, one tornado was spawned in the Czech Republic in the late evening hours (Setvak, 2000).

The hailstorm studied in the present paper was the right–mover of a storm splitting at about 1645 UTC over the Allgäu region in southern Germany. While the left–moving cells decayed

very quickly, the right–moving cell (heading in an easterly direction within the mid–level flow from south–west) intensified very rapidly and developed supercell characteristics such as a single persistent updraft, a bounded weak echo region, an echo overhang and mid–level mesocyclonic rotation (Höller et al., 1999b, 2000). In the vicinity of the cumulonimbus cell, other active thunderstorms were also present in the observation area which was centered in Oberpfaffenhofen and extended about 60 km in each horizontal direction (cf. Fig. 1).

From 1700 UTC on, the young supercell storm approached the experimental area around Oberpfaffenhofen. The onset of lightning activity was monitored both by the LPATS system and the two ITF stations at Oberschleißheim (northern) and Wielenbach (southern) operated by ONERA. The latter station was equipped with the elevation sensor allowing for a three–dimensional reconstruction of the location of lightning VHF emissions.

Fig. 2 shows the flash rate measured by the ITF sensors, both for the whole area (solid line) and the region of the supercell alone (lower shaded area). While before 1430 UTC no lightning flashes were observed (as well as after 2200 UTC), it is obvious from the early peak in flash rate at 1630 UTC that there was considerable thunderstorm activity in the area before the supercell originated from its parent cell. In our analysis we focus on the time period 1700–2000 UTC which contains the intensification phase (up to 1800 UTC), the mature stage (up to about 1830 UTC) and the subsequent decay of the storm into a multicell complex. Coincidentally, the supercell passed right over the southern ITF–station between about 1800–1815 UTC, already slightly weakening. We see from Fig. 2 that the flash rate during the most vigorous phase of the storm exceeded 40 min^{-1} and seldom fell below 30 min^{-1}. Note the rapid rise of the flash rate after 1730 UTC. The minimum around 1815 UTC was likely an artifact caused by the passage over the ITF sensor and not due to a genuine decrease of lightning activity. After 1930 UTC almost all measured lightning flashes originated from the storm studied here.

Considering the radar data, the most noticeable cloud growth and internal organization took place between 1730 UTC and 1800 UTC, accompanied by the large rise in flash rate. The according radar–observed echo tops in km AGL are depicted by the numbers atop the curves in Fig. 2 from 1730 to 1833 UTC. Obviously the flash rate rose simultaneously to the increase in cloud top height. The storm was tracked by POLDIRAD sector volume scans repeated every few minutes and additional range–height indicator (RHI) and plan position indicator (PPI) scans.

Fig. 3 shows three sections through the storm at 1757 UTC near the point of maximum

cumulonimbus development. The lower left panel of the figure gives the constant–altitude PPI (CAPPI) at 5.5 km AGL, while the upper left and lower right panels depict x,z and y,z vertical slices at $x = -16.5$ km and $y = -27.5$ km distance from POLDIRAD, respectively. Section location is denoted by the thin lines in the panels. The x,z–diagram shows a large echo overhang and a weak echo region below. This corresponds to the region of the updraft with inflow of lower–level air and is also visible in the CAPPI south–east of the reflectivity core or in the Doppler velocity (cf. Höller et al., 1999b, 2000). Other characteristics indicating supercell dynamics for this hailstorm were the presence of a mesocyclone in mid–levels and the persistence of the single main updraft for some tens of minutes.

The cumulonimbus system lost its supercell structure after about 1845 UTC and was then better characterized as a multicell storm with some phases of re–intensification due to the development of new cells (cf. also Fig. 2).

3 Vertical structure of VHF activity

Both theoretical (Williams, 1989; Saunders, 1993) and also experimental results (Simpson & Scrase, 1937; Rison et al., 1999; Solomon et al., 1999) indicate that the charge accumulation in a thunderstorm can, in many cases, be modeled by a negative charge center around the $T = -15 \pm 10^\circ$ C level and an upper positive charge center near the $T = -35 \pm 10^\circ$ C level within mature cumulonimbus clouds. A smaller lower positive charge region can sometimes be found close to the freezing level (Williams, 1989). This three–level conceptual model is known as the tripole model of thunderstorm electrification. However, as shown by Stolzenburg et al. (1998a,b,c) this tripole structure is neither a universal feature of all thunderstorms nor universally present in all regions of single storms. Nevertheless, the tripole concept was chosen as a test basis for the EULINOX data analysis.

In order to compare our findings with the tripole model within the synoptic setting of 21 July 1998 we have to assess the heights of the three temperature levels. On that day, maximum temperatures near the ground level ranged between 25° C and 35° C. As can be deduced from a composite afternoon vertical sounding (Fehr, 2000), the height of a negative charge center can be expected to be within 5 and 7.5 km AGL, and an upper positive charge center approximately 3 km higher up, i. e. at a height of about 8 to 10 km AGL. These regions are indicated in Fig. 4 by the hatched areas.

3.1 Vertical profiles

As a first step the gridded ITF data are evaluated in order to detect distinct peaks in vertical profiles of VHF source density to look for evidence of any charge centers predicted by the tripole model. Within the above mentioned ring–shaped area ranging between 10 km and 25 km around the southern ITF station Wielenbach vertical profiles of VHF sources integrated over 3 min intervals and a 1 km^3 grid have been analyzed. The 15 grid layers in the vertical z–direction are located at heights of 0.5, 1.5, . . . , 14.5 km AGL. In order to detect only distinct peaks in the vertical VHF profile at a given horizontal position within the grid, the following conditions must be met: i) the profile data must not be sparse, i. e. the total number of VHF sources in the profile should exceed the number of 15 vertical grid points, ii) the number of VHF sources at the peak level must exceed 15 % of the total number of VHF sources in the profile, iii) the vertical distance between consecutive peaks must exceed the vertical grid spacing to assure that plateaus in the profiles are not erroneously classified as two separate peaks.

During the time period considered (1700 to 2000 UTC), most vertical profiles for which distinct peaks could be identified were single–peak profiles (666 cases). In another 204 cases, two peaks were found, and in only 24 cases three maxima were detected using the above conditions. However, the vast majority of vertical profiles does not show any distinct maximum of VHF activity, mostly due to data sparseness of the profiles.

Owing to the fact that the gridded data only allowed for analysis of bulk structures in the vertical profiles due to the 1 km spatial resolution, the vertical grid columns of VHF emissions were subjected to an averaging process. However, averaging all VHF profiles within the ring around Wielenbach only yielded one maximum of VHF activity located at 3.5 km AGL, i. e. near the freezing level. Any upper level maximum, if present below 11 km AGL, was suppressed by the averaging procedure. Yet as observations and theory predict clearly distinguishable charge layers at least in certain parts of a thundercloud one could expect that for most two–peak vertical profiles these peaks are located at similar altitude levels. In addition, one–peak profiles should also reproduce one of the predicted charge layers and so their peak level should coincide with one of the peak levels in multi–peak VHF profiles. To test this hypothesis the vertical profiles were averaged in a different way: one and two–peak profiles were averaged separately. The 24 three–peak profiles, however, did not provide a statistically significant basis suitable for averaging.

The result of this separate averaging is depicted in Fig. 4. The dashed line gives the average

of all one–peak profiles and the solid line the average of the two–peak profiles. In both cases the low–level maximum at 3.5 km AGL is most pronounced. The solid curve, however, shows a secondary maximum at 6.5 km AGL which corresponds to the –15° C level of 21 July 1998. Yet in neither of the average profiles do we find an upper–level maximum near the –30° C region inside the cloud where we would expect the main positive charge level of a cumulonimbus tripole. There are of course VHF sources at that level, but not enough to form a distinguishable peak. Instead the peak near the freezing level dominates all profiles (even an average of all sparse profiles without distinct peaks leads to a flat maximum at that level).

We noticed that this low–level maximum is due to an unusually high number of low–altitude intracloud negative leaders during this storm. The negative leader, as observed by the ITF, is characterized by a succession of sources, and propagates towards or inside a positive charge region. In other storms we surveyed, most of negative leaders were the downward leader of negative cloud–to–ground flashes, or in some cases mid–altitude intracloud leaders, and we often noticed that these intracloud negative leaders had a less intense VHF emission than downward leaders. This can be explained by a pressure–dependent behavior of the negative leader causing more frequent and more intense VHF emissions at higher ambient air pressure (Lalande & Bondiou–Clergerie, 1997). Consequently, the high VHF emissivity of some intracloud negative leaders during the 21 July 1998 storm can be due to their low altitude just above cloud base. They may have propagated inside a highly developed low–level positive charge center. So we might argue that such an unusually large number of low–level negative leaders in the EULINOX storm could be the source of the dominant low–altitude peak in the mean VHF profiles. Therefore even the weaker secondary maximum noticeable in Fig. 4 is no longer present in an average over all vertical profiles.

3.2 Single flashes

The intracloud flash from the growing storm at 1737 UTC shown in Fig. 5 gives a very instructive impression of the intracloud lightning activity of this EULINOX storm. This flash and many others come very close to the basic view of intracloud lightning presented in MacGorman & Rust (1998, p. 203) as well as other measurements (Shao & Krehbiel, 1996; Rison et al., 1999; Solomon et al., 1999). The distribution of VHF sources in the vertical depicted in the small panel of Fig. 5 shows two distinct maxima at about 6.5 km and 9 km AGL. The upper peak is more prominent than the lower one. These levels correspond to about the –30° C and the

–15° C altitudes. While the lower VHF region shows little vertical variation from one end of the flash to the other, the layer of upper–level VHF activity gradually rises from 8 km at the eastern edge to 11 km AGL at $x \simeq -32$ km before it descends again to about 8 km at the western end of the intracloud lightning. However, some care has to be taken because near the western end of the flash the points from the upper and the lower level come very close to each other. So a clear distinction between the two levels is no longer possible in this region.

Nevertheless this rise and fall of the upper distribution of VHF sources is in satisfactory agreement with the approximate location of the updraft core within the strongly developing supercell at that time. The location of the greatest altitude in this flash is close to the downshear edge of the updraft while the edges of the flash are located farther away from the updraft core near $(x, y) \simeq (-32, -28)$ km. As pointed out by Stolzenburg & Marshall (1998) and Williams (1989, cf. Fig. 3 therein), the upper positive charge layer is more easily affected by the storm's dynamics which can therefore lead to larger variations in VHF signal altitude throughout the cumulonimbus cloud. The negatively charged region around the –15° C level, however, remains less affected by such changes in updraft strength, just as the VHF sources there. In this region near the cumulonimbus cell's main updraft the phenomenon might be interpreted in the following way: charge separation leads to positively charged small ice crystals in the upper part of the cloud and negatively charged larger hydrometeors at intermediate levels (cf. Saunders, 1993). Due to their small terminal velocity, the floating ice crystals higher up (+) can respond to variations in vertical air motions much easier compared to the larger particles beneath (−), cf. Williams (1989). Furthermore, the slowly falling ice crystals can be advected at nearly constant altitude by the horizontal wind even without supporting updrafts. On the other hand, horizontal advection of larger particles for longer distances at constant height requires a distinct range of supporting updraft speeds, which generally are not observed in storms. This can serve as a possible explanation for the impression from Fig. 5 that the upper region of VHF sources is more horizontally widespread and more continuous than the lower one.

4 Lightning activity and cloud microphysics

After evaluation of the VHF interferometer results we now incorporate the C–band polarimetric Doppler radar measurements. This provides information on the coupling between cloud microphysics and lightning discharges necessary for developing parameterizations for mesoscale or

global models. Aside from the vertical profile of VHF activity studied before, modellers would need to relate flash location and flash rate to prognostic variables of their model, or quantities derived from these variables. One of these quantities is the radar reflectivity factor Z which itself is a function of hydrometeor content. As it can readily be computed from the output of mesoscale cloud models it would be welcome to find a clear relationship between lightning activity and reflectivity factor.

In this context it was found that the region of high VHF activity typically was shifted away from the reflectivity core of the supercell storm. The shift was mostly to the left downshear side of the storm's center, i. e. on the northern flank of the east–moving storm. To obtain information on the correlation between number of VHF sources N_{VHF} and reflectivity factor Z, the volume data measured by the radar at 1730, 1745, 1757, 1809, 1821, and 1833 UTC were related to the total number of VHF sources within 3 min periods starting at the six given volume scan times. As the radar data were interpolated onto the same 1 km^3 grid as used for the ITF data, the points could directly be analyzed from a scatter plot of N_{VHF} versus Z.

This is shown in Fig. 6 a for the growing phase of the storm (1730, 1745 UTC) as well as its early decaying stage in Fig. 6 b (1821, 1833 UTC). In all four volume scans the highest observed reflectivities interpolated to the cartesian 1 km^3 grid were in the range from 50 to 52.5 dBZ. In the developing stage of the storm, no VHF data points are found for Z $\gtrsim$ 43 dBZ. Instead, weak VHF activity is found with usually less than 10 VHF sources per 3 min interval and per km^3. The peak number of 12 VHF sources per point is located at roughly 32 dBZ. The decrease in number of sources from the maximum towards lower reflectivity factors is slower than that for higher Z–values. This skewness towards higher reflectivity factors is also found during the decaying stage of the storm. But quantitatively the differences are large: the reflectivity within grid boxes with VHF sources now extends up to about 52 dBZ and the VHF activity itself also has increased substantially: many grid boxes contain 10 or more sources per 3 min interval and per km^3 with a peak value of 30. In addition, the location of this maximum has shifted towards higher reflectivity factors. Instead of 32 dBZ in the early stage, the scatter plot now peaks at 45 dBZ and then drops off very rapidly with increasing Z. The data are more strongly skewed than before, but in general the shapes of the two scatter–data sets seem to bear a similarity, because the data region of 1730 and 1745 UTC coincides with the left flank of the data region at 1821 and 1833 UTC. As a consequence, for Z $<$ 25 dBZ the number of VHF signals is always less than 5.

This observed behavior during supercell evolution indicates that either a change in concentration or in size / type of the lightning–related hydrometeors must have taken place. The concentrations were not directly measured and can only be inferred from the polarimetric radar data with considerable uncertainties. So here we focus on the second alternative and inspect wether there are different preferred hydrometeor regions with lightning discharges in different stages of the storm. In addition we can evaluate which of these regions has the highest specific VHF emissions per unit time and unit volume.

To identify which hydrometeors were related to lightning activity in the EULINOX supercell the hydrometeor classification scheme developed by Höller et al. (1994) and Höller (1995) was used to compute the dominant hydrometeor types in the radar scan volume from the polarimetric radar data Z, ZDR, LDR, thereby taking into account particle size, shape and surface (dry / wet) characteristics. The classes of Höller's scheme are summarized in Tab. 1. For clarity the twelve hydrometeor categories are further merged into three main hydrometeor groups: cloud, rain (classes 0–2, 5), graupel (classes 3 and 4), and hail (classes 6–11).

Fig. 7 shows different time series of these hydrometeor groups from 1730–1833 UTC. In Fig. 7 a the total volume of each hydrometeor group is given as the number of 1 km^3 grid boxes dominated by this hydrometeor type. During cloud growth the graupel volume is largest, and only after 1800 UTC the hail volume starts to increase by a factor of three while the graupel volume strongly decreases. In late stages of the supercell the hail volume is larger than that of the graupel region. Fig. 7 b gives the total number of VHF sources observed in 3 min intervals in the three hydrometeor regions. The curves are similar in shape to Fig. 7 a and confirm theoretical predictions claiming graupel pellets to be the best candidates for a high correlation with lightning discharges. Yet again, this only holds in the growing and mature stages of cumulonimbus development. After 1800 UTC VHF emissions from the hail core quickly rise and surpass those from the graupel region from 1810 UTC on. This also yields an explanation for the changes from Fig. 6 a to Fig. 6 b: Most lightning discharges now occur near large hydrometeors (hail and probably also heavy rain) resulting in large values of the reflectivity factor.

Looking at the specific VHF emissions from the three hydrometeor groups, i. e. dividing the number of sources from Fig. 7 b by the number of grid boxes from Fig. 7 a, one sees that for cloud, rain and graupel this specific ratio is roughly constant with time. For hail, however, this average ratio rises after 1800 UTC from roughly 2 to about 4 at 1821 and 1833 UTC. This supports the higher peak in Fig. 6 b and shows that in late stages of cloud development the

hail core and the heavy precipitation shaft are quite effective producers of lightning discharges. One can speculate that some percentage of the charged graupel pellets will be transformed to hailstones during cloud evolution and so contribute to the space charge in the hail core. But the exact reason why during late storm evolution hail is specifically more effective than other hydrometeors in producing discharges is not obvious.

After this analysis it is worthwhile to look at the spatial distribution of lightning discharges as observed by the ITF. Fig. 8 was computed from the radar volume scan and the VHF volume data on the 1 km^3 cartesian grid at 1757 UTC (similar to Fig. 3 taken from the same point in time) close to the stage of maturity of the EULINOX supercell storm on 21 July 1998. The greyscale code represents the main hydrometeor groups of Fig. 7 based on the classification shown in Tab. 1. The diagram shows three sections through the radar volume: a CAPPI and two RHIs in x,z and y,z planes, respectively. The location of the sections is given by the thin solid lines in the figure and was chosen to show regions with as many VHF signals as possible. One can draw the conclusion from this diagram that the VHF activity is mainly linked to the hydrometeor classes 3 and 4: mainly graupel, to a lesser degree snow and small dry hail. Similar pictures from the other available radar volume data (not shown here) further support this observation already gained from Fig. 7. The vertical sections hardly indicate a tendency for horizontal layering of VHF emissions near the temperature levels predicted by the tripole concept: 3.5 km, 6 km, and 9 km AGL. It is apparent that any layered structures are only established in specific downshear regions of the cloud. The tripole model definitely cannot be valid everywhere inside the cloud, especially in regions of very strong up and downdrafts such as the storm's core at (–18, –30) km (cf. Stolzenburg et al., 1998a).

This diagnosis is corroborated by Fig. 9 focusing on the graupel region inside the storm. This radar image offers a closer look at the vertical structure of individual lightning discharges (Höller et al., 1999b, 2000). Fig. 9 is an RHI at 231° azimuth from POLDIRAD in Oberpfaffenhofen at 1741 UTC, when the supercell was still strongly developing. Here only the graupel field (shaded) as derived from the Höller scheme is shown together with nearby individual VHF bursts (line segments and crosses) occurring within a ± 30 s time and $\pm 10°$ azimuth window around the RHI scan. Again the majority of VHF sources is found in the graupel zone, few signals belong to the hail core (to the right of the graupel region) and the snow region downshear in the anvil (to the upper left of the graupel field). Here no horizontal layering of the lightning discharges can reliably be diagnosed. Instead the VHF sources group vertically among the

graupel particles, leading to a waterfall–like structure on the downshear side of the east–moving updraft core.

A reason for this might be inferred from Ziegler & MacGorman (1994) and Stolzenburg et al. (1998a, Figs. 8 and 9 therein): the graupel pellets are negatively charged while floating within the updraft. As soon as they start to fall out on the downshear flank of the updraft, the charge layer plunges and due to the smaller distance of the now oblique charge regions the electromagnetic field can become strong enough to initiate lightning discharges.

5 Discussion

The results obtained yield an instructive view of the 21 July 1998 EULINOX supercell storm. Some theoretical predictions could already be corroborated by combination of VHF interferometry and polarimetric Doppler radar measurements. The three–dimensional information on cloud structure and lightning activity gathered by these two systems provided some evidence for charge separation due to the riming graupel–ice crystal interaction mechanism within the updraft core of the growing thundercloud. Theoretical and experimental work (Williams, 1989; Williams et al., 1989; Saunders, 1993; Brooks et al., 1997; Stolzenburg & Marshall, 1998; MacGorman & Rust, 1998; Takahashi et al., 1999) had predicted this close relation between lightning and graupel, but only the three–dimensional overlay of radar and ITF data allowed analysis of the zones inside the cloud where discharges were more or less horizontally layered or formed structures vertically aligned downshear of the main updraft. In both cases most of the lightning discharges occurred in regions with graupel pellets.

In this study we have also treated temporal changes of the lightning–microphysics coupling during growth, maturity, and decay of the EULINOX hailstorm. In addition to the results presented by Dotzek et al. (2000b) a significant change in discharge–related hydrometeor types after storm maturity could be substantiated: instead of graupel pellets now the hail core appears to be the main source of lightning VHF emissions. This explains the observed shift towards higher reflectivity factors in the scatter plot of Fig. 6 b and is further coupled with a higher specific VHF emission per unit time and volume compared to that of the graupel region. The exact physical processes leading to these observed effects are presently being investigated.

Compared to the lightning–hydrometeor coupling, for the vertical structure of lightning activity the results are less unequivocal: in some parts of the cloud VHF signatures showing a

preference for horizontal layers appeared to be present, while in other parts no evidence of even a convincing dipole structure could be detected. With Rust & Marshall (1996) and Stolzenburg et al. (1998a,b,c) we state here that the real structure of thunderstorms is far more complex than the simple tripole concept, even though the physical processes postulated in the tripole model are likely to be present in parts of the thundercloud.

Finally, a puzzling feature remains to be addressed: the strong VHF activity near the freezing level within this supercell storm. This could indicate that the lower (secondary) positive charge layer of the cumulonimbus cloud was overwhelmingly active in this special case. Physical evidence for this assumption is given by Williams (1989) and Saunders (1993): it could be due to a reversal of the sign of charge acquired by the graupel as it falls into a warmer zone with higher liquid water content. Or it could come from the charge transport from intracloud flashes that brought positive charge to the main negative charge center and then on to lower levels. In a different context Shepherd et al. (1996) also observed strong electric fields and charges near the melting layer in the stratiform part of mesoscale convective systems. The authors argue that a melting–charging mechanism could be responsible for that.

On the other hand the low–level negative leaders which were found in the data from the EULINOX supercell are likely to be highly prominent in VHF due to the larger air pressure at this low altitude (Lalande & Bondiou–Clergerie, 1997). Thus they tend to enhance the VHF signatures of lightning activity there. However, the present investigation was focused on the higher levels inside the cumulonimbus cloud and on bulk statistics of cloud microphysics and cloud electricity. Future analysis of other EULINOX storms of different type will possibly further clarify the processes that govern cloud electricity near the freezing level. This would also be desirable from the standpoint of flight safety (Pike, 2000).

6 Conclusions

During the intensive observation period of the EULINOX campaign in southern Germany during the summer of 1998 detailed measurements with an unprecedented variety of measuring platforms were being undertaken to clarify the NO_X production due to lightning discharges within thunderstorms. Both from the standpoints of cloud chemistry and microphysics the results have proven to be very fruitful.

In summary, from the analysis of the radar and ITF data collected from the 21 July 1998

EULINOX supercell storm event we conclude the following:

1. cloud microphysical aspects of thunderstorm electricity could effectively be studied with the combination of a polarimetric radar and a VHF lightning mapper,

2. in some parts of the cumulonimbus cloud, lightning flashes were linked to certain height regions, weakly resembling the upper positive charge center, the negative region around the –15° C altitude, and a lower positive charge layer near the freezing level,

3. these charge layers were not generally detectable inside the cloud, especially not in regions where strong convective motions dominate the cumulonimbus dynamics. Moreover, all three layers did not always exist simultaneously,

4. the strong lower positive charge center near 0° C appears to be a peculiarity of this supercell storm,

5. during cloud growth most VHF lightning signals were found in the storm regions where graupel pellets (as inferred from polarization diversity radar) dominated, while during cloud decay VHF sources were increasingly emitted from hail and heavy rain regions.

Studying other cases of the EULINOX campaign will deepen the insight in the physics of lightning, not only within supercells, but for a variety of other storm types as well.

Acknowledgments

This work was partly funded by the Commission of the European Communities under contract No. ENV4–CT97–0409. Thanks to Martin Hagen and Heidi Huntrieser for many fruitful discussions and to an anonymous referee for valuable comments.

Information on the LINOX and EULINOX campaigns can be obtained from the web sites http://www.pa.op.dlr.de/linox/ and http://www.pa.op.dlr.de/eulinox/.

References

Brooks, I. M., C. P. R. Saunders, R. P. Mitzeva, S. L. Peck, 1997: The effect on thunderstorm charging of the rate of rime accretion by graupel. *Atmos. Res.* **43**, 277–295.

Defer, E., 1999: *Caractérisation et modélisation de l'activité électrique de nuages d'orage.* Ph. D. thesis, Univ. Paris VII, 233 pp.

Dotzek, N., H. Höller, C. Théry, 2000a: *VHF–interferometry and radar observation: Implications for nitrogen oxides production*. In: EULINOX — final report, DLR Forsch. Ber. 2000–28, Cologne, 240 pp. [http://www.op.dlr.de/~pa4p/papers.htm]

Dotzek, N., H. Höller, C. Théry, 2000b: Lightning and microphysics in a EULINOX supercell storm. *Phys. Chem. Earth* B **25**, 1285–1288. [http://www.op.dlr.de/~pa4p/papers.htm]

Fehr, T., 2000: *Mesoskalige Modellierung der Produktion und des dreidimensionalen Transports von Stickoxiden in Gewittern*. Ph. D. thesis, Univ. Munich, 116 pp. [http://www.op.dlr.de/~pa10/PhDsite.html]

Höller, H., 1995: Radar–derived mass–concentrations of hydrometeors for cloud model retrievals. *Proc. 27th Conf. on Radar Meteor.*, Vail, 453–454.

Höller, H., V. N. Bringi, J. Hubbert, M. Hagen, P. F. Meischner, 1994: Life cycle and precipitation formation in a hybrid–type hailstorm revealed by polarimetric and Doppler radar measurements. *J. Atmos. Sci.* **51**, 2500–2522.

Höller, H., U. Finke, H. Huntrieser, M. Hagen, C. Feigl, 1999a: Lightning–produced NO_X (LINOX): Experimental design and case study results. *J. Geophys. Res.* **104** D, 13 911–13 922.

Höller, H., P. Laroche, M. Hagen, J. Seltmann, U. Finke, 1999b: Radar and lightning structures of thunderstorms during EULINOX. *Proc. 29th Conf. on Radar Meteor.*, Montreal, 611–612.

Höller, H., T. Fehr, C. Théry, J. Seltmann, H. Huntrieser, 2000: Radar, lightning, airborne observations, and modelling of a supercell storm during EULINOX. *Phys. Chem. Earth* B **25**, 1281–1284.

Huntrieser, H., H. Schlager, C. Feigl, H. Höller, 1998: Transport and production of NO_X in electrified thunderstorms: Survey of previous studies and new observations at mid–latitudes. *J. Geophys. Res.* **103** D, 28 247–28 264.

Lalande, P., A. Bondiou–Clergerie, 1997: Collection and analysis of available in–flight measurement of lightning strikes to aircraft. *Final report of Fulmen European Project on Analysis of Experimental data and models for upgraded lightning protection requirements*, DG VII, Transport Research and Technological Development Programs. Rep. Al–95–SC.204–RE / 210–D:1.

Lee, D. S., I. Köhler, E. Grobler, F. Rohrer, R. Sausen, L. Gallardo–Klenner, J. G. J. Olivier, F. J. Dentener, A. F. Bouwman, 1997: Estimates of the global NO_X emissions and their uncertainties. *Atmos. Env.* **31**, 1735–1749.

MacGorman, D. R., W. D. Rust, 1998: *The Electrical Nature of Storms*. Univ. Press, Oxford, 422 pp.

Pike, W. S., 2000: A note on some recent lightning strikes to aircraft which were either climbing or descending through the freezing level in or near hail–producing cumulonimbus cloud. *J. Meteor.* **25**, 109–116.

Rison, W., R. Scott, R. J. Thomas, P. R. Krehbiel, T. Hamlin, J. Harlin, 1999: 3–dimensional lightning and dual–polarization observations of thunderstorms in central New Mexico. *Proc. 11th Int. Conf. on Atmos. Electricity*, Huntsville, 432–435.

Rust, W. D., T. C. Marshall, 1996: On abandoning the thunderstorm tripole–charge paradigm. *J. Geophys. Res.* **101** D, 23 499–23 504.

Saunders, C. P. R., 1993: A review of thunderstorm electrification processes. *J. Appl. Meteor.* **32**, 642–655.

Setvak, M., 2000: Pers. comm. *1st Conf. on European Tornadoes and Severe Storms*, Toulouse.

Shao, X.–M., P. R. Krehbiel, 1996: The spatial and temporal development of intracloud lightning. *J. Geophys. Res.* **101** D, 26 641–26 668.

Shepherd, T. R., W. D. Rust, T. C. Marshall, 1996: Electric fields and charges near 0° C in stratiform clouds. *Mon. Wea. Rev.* **124**, 919–938.

Simpson, S. G., F. J. Scrase, 1937: The distribution of electricity in thunderclouds. *Proc. Roy. Soc. London* A **161**, 309–352.

Solomon, R., C. Théry, E. Defer, A. Bondiou–Clergerie, 1999: Thunderstorm and lightning development: modeling and observations. *Proc. 11th Int. Conf. on Atmos. Electricity*, Huntsville, 335–338.

Stolzenburg, M., T. C. Marshall, 1998: Charged precipitation and electric field in two thunderstorms. *J. Geophys. Res.* **103** D, 19 777–19 790.

Stolzenburg, M., W. D. Rust, B. F. Smull, T. C. Marshall, 1998a: Electrical structure in thunderstorm convective regions. 1. Mesoscale convective systems. *J. Geophys. Res.* **103** D, 14 059–14 078.

Stolzenburg, M., W. D. Rust, T. C. Marshall, 1998b: Electrical structure in thunderstorm convective regions. 2. Isolated storms. *J. Geophys. Res.* **103** D, 14 079–14 096.

Stolzenburg, M., W. D. Rust, T. C. Marshall, 1998c: Electrical structure in thunderstorm convective regions. 3. Synthesis. *J. Geophys. Res.* **103** D, 14 097–14 108.

Takahashi, T., T. Tajiri, Y. Sonoi, 1999: Charges on graupel and snow crystals and the electrical structure of winter thunderstorms. *J. Atmos. Sci.* **56**, 1561–1578.

Théry, C., 2000: *Evaluation of LPATS data using VHF interferometric observations of lightning flashes during the EULINOX experiment*. In: EULINOX — final report, DLR Forsch. Ber. 2000–28, Cologne, 240 pp.

Théry, C., P. Laroche, P. Blanchet, 2000: *Lightning activity during EULINOX and estimation of NO_X production by flashes*. In: EULINOX — final report, DLR Forsch. Ber. 2000–28, Cologne, 240 pp.

Williams, E. R., 1989: The tripole structure of thunderstorms. *J. Geophys. Res.* **94** D, 13 151–13 167.

Williams, E. R., M. E. Weber, R. E. Orville, 1989: The relationship between lightning type and convective state of thunderclouds. *J. Geophys. Res.* **94** D, 13 213–13 220.

Ziegler, C. L., D. R. MacGorman, 1994: Observed lightning morphology relative to modeled space charge and electric field distribution in a tornadic storm. *J. Atmos. Sci.* **51**, 833–851.

Tables

Table 1: Hydrometeor classification scheme after Höller et al. (1994) and Höller (1995). Classes 0–2, 5 (cloud, rain), 3–4 (graupel), and 6–11 (hail) form main hydrometeor groups (cf. Figs. 7 and 8).

Index	Hydrometeor Type
0	Thin cloud (no classification)
1	Small raindrops
2	Rain
3	Small graupel, snow
4	Large graupel (dry), small hail (dry)
5	Rain, small hail (wet)
6	Hail (dry)
7	Hail (wet)
8	Large hail (porous, wet)
9	Large hail (wet)
10	Rain and large hail (wet)
11	Rain and hail

Figure captions

Figure 1: Map of EULINOX main observation area. The operation center at DLR in Oberpfaffenhofen is given by the + symbol, the two ITF sensors are shown as ◇ symbols. Two circles mark the 10 km and 25 km range from the southern ITF sensor at Wielenbach.

Figure 2: Flash rate for the supercell (lower filled curve) and the total observation area (upper solid curve) in the time period 1530–2200 UTC measured by the ITF sensor. Numbers atop the curves give the supercell radar echo top in km AGL from 1730–1845 UTC.

Figure 3: Radar reflectivity factor Z for a horizontal section (CAPPI) and two vertical sections (RHI) through the storm at 1757 UTC. The thin lines give the location of the cross sections.

Figure 4: Average (1700–2000 UTC) vertical profiles of 666 VHF columns containing one distinct maximum (dashed) and 204 VHF columns containing two (solid). The hatched height ranges mark expected probable locations of main charge layers and their polarity according to the tripole model on 21 July 1998.

Figure 5: Projection of a high–altitude IC flash. Each symbol corresponds to one VHF source mapped by the ITF sensor. Dashed lines denote the elevation limits of the ITF. The small panel gives height distribution of VHF signals.

Figure 6: Scatter plot of VHF sources per 3 min interval km^{-3} and radar reflectivity factor Z for 1730, 1745 UTC (a, growing stage) and 1821, 1833 UTC (b, decaying stage).

Figure 7: Time series of number of 1 km^3 grid boxes (a) and VHF sources per 3 min (b) related to three main hydrometeor groups derived from six POLDIRAD volume scans.

Figure 8: Main hydrometeor groups (cf. Tab. 1 and Fig. 7) for one horizontal (CAPPI) and two vertical sections (RHI) through the storm at 1757 UTC. Location of the sections is depicted by thin lines. Crosses mark VHF activity in 1 km^3 grid boxes between 1757 and 1800 UTC.

Figure 9: RHI at 231° azimuth showing the graupel region (shaded) in the rapidly growing cloud at 1741 UTC. Nearby (± 30 s, $\pm 10°$ azimuth) discharges are given by crosses and lines.

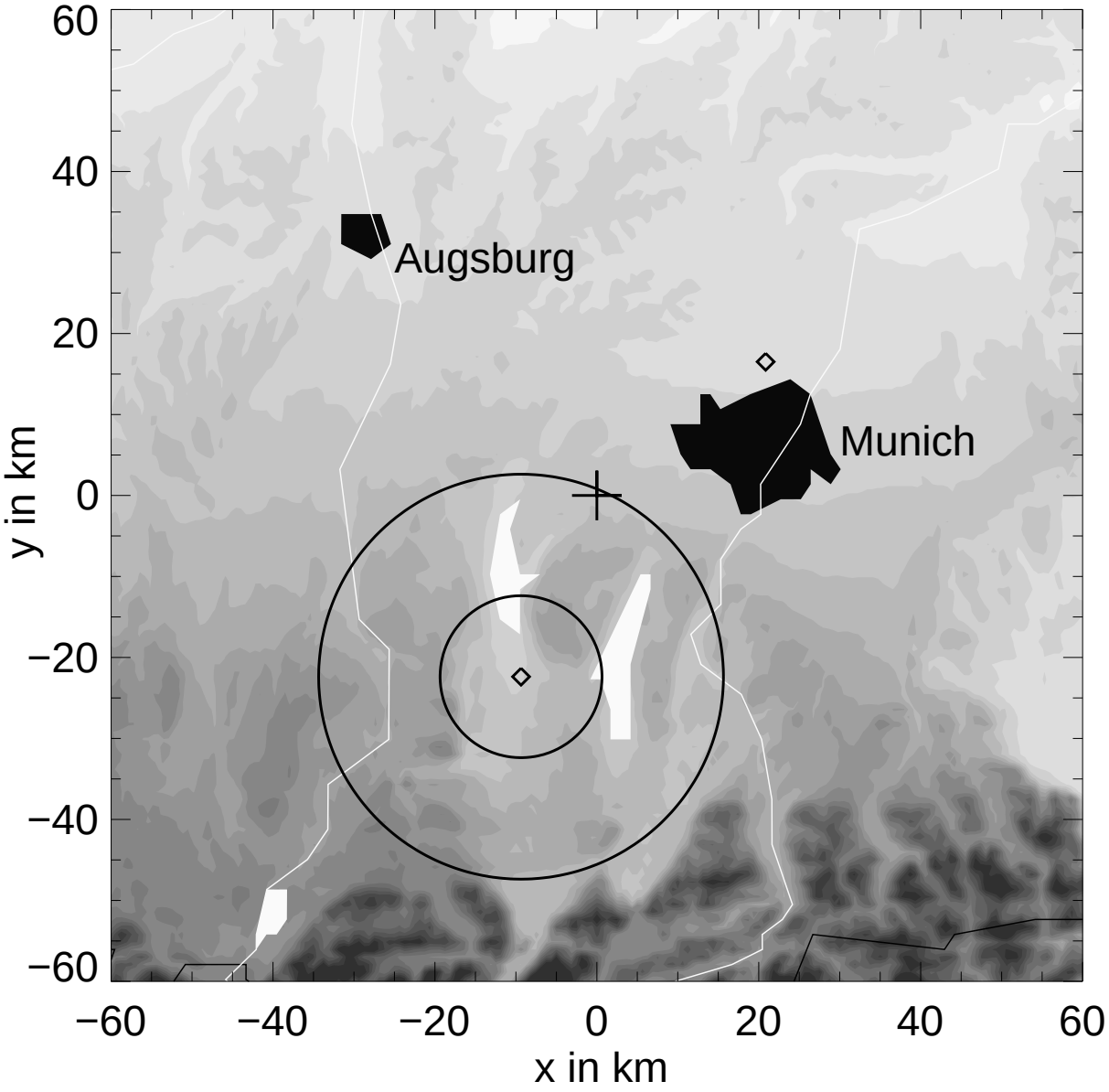
Augsburg
Munich
60
40
20
0
−20
−40
−60
y in km
−60
−40
−20
0
20
40
60
x in km

Figure 1

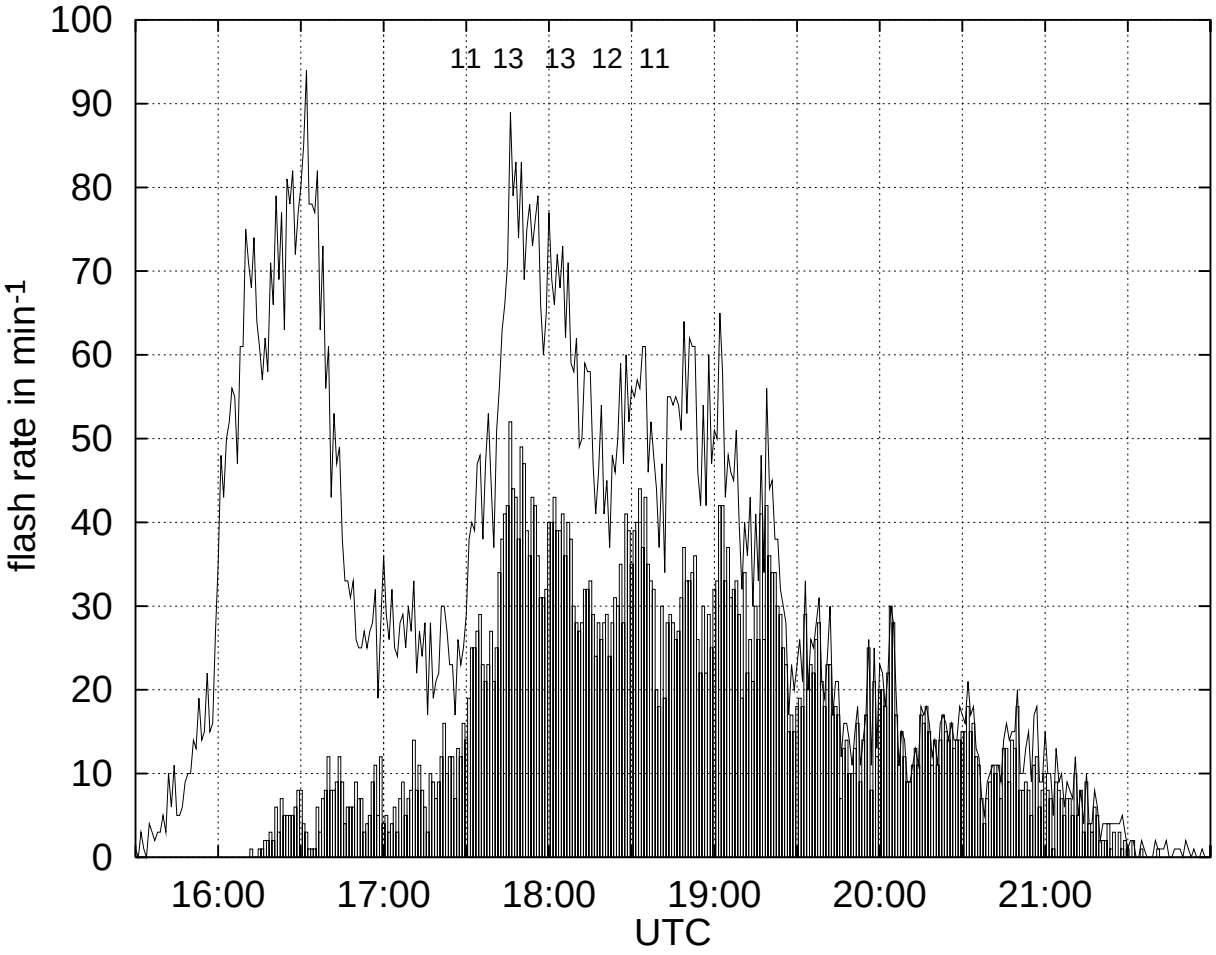
11 13 13 12 11
flash rate in min-1
UTC
0
10
20
30
40
50
60
70
80
90
100
16:00
17:00
18:00
19:00
20:00
21:00

Figure 2

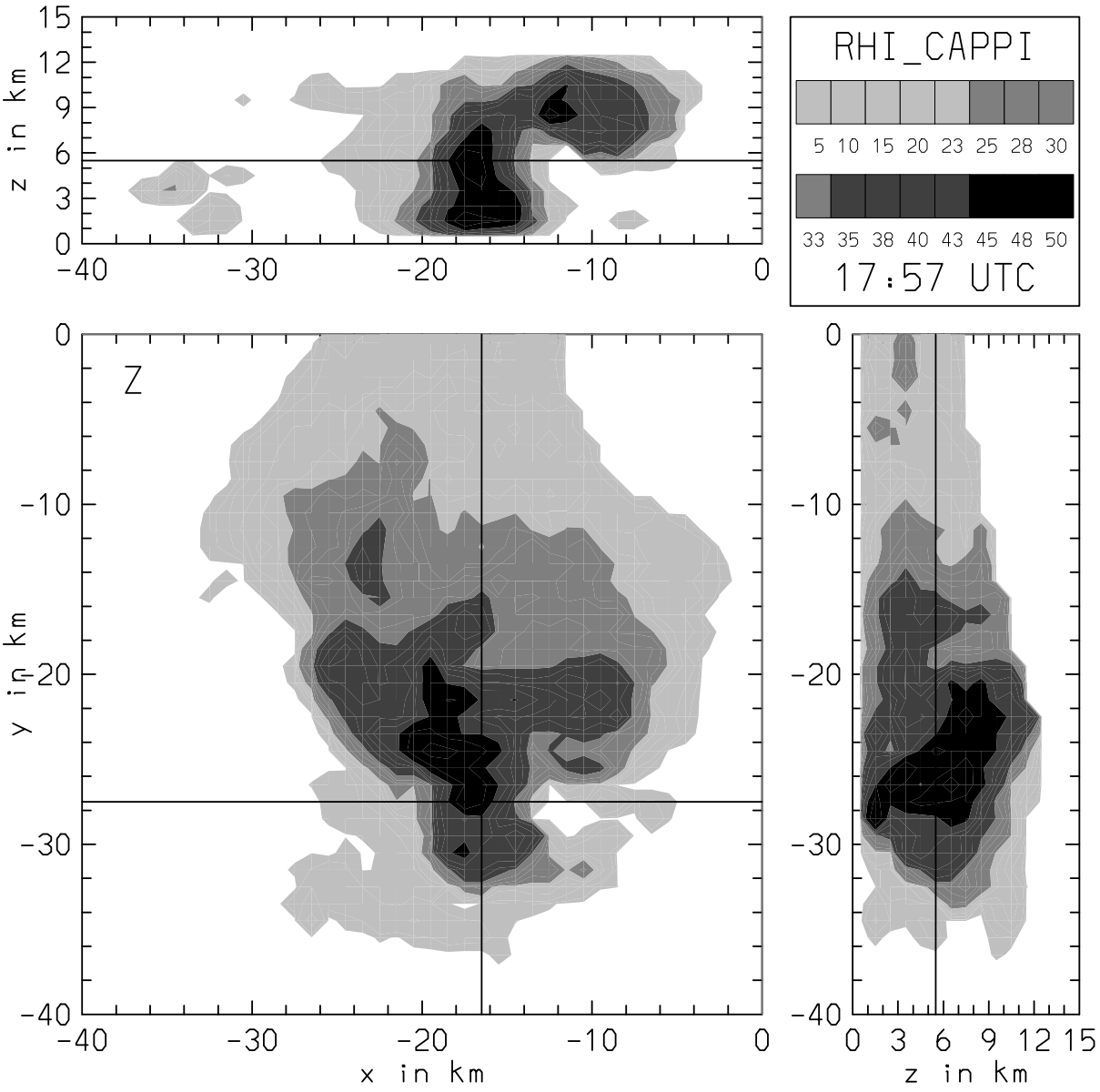
RHI_CAPPI
5 10 15 20 23 25 28 30
33 35 38 40 43 45 48 50
17:57 UTC
z in km
Z
y in km
x in km
z in km

Figure 3

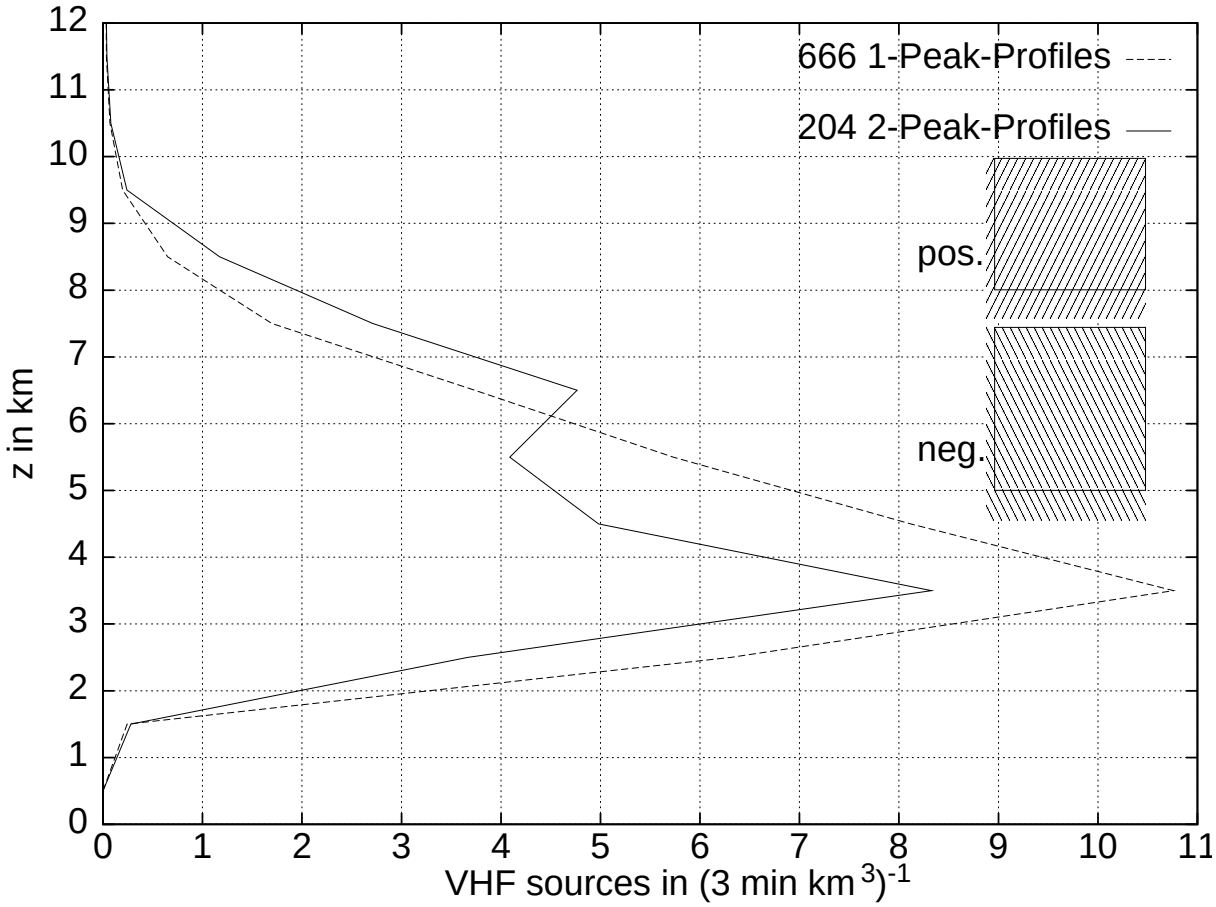
666 1-Peak-Profiles
204 2-Peak-Profiles
pos.
neg.
z in km
VHF sources in (3 min km 3)-1
0
1
2
3
4
5
6
7
8
9
10
11
12

Figure 4

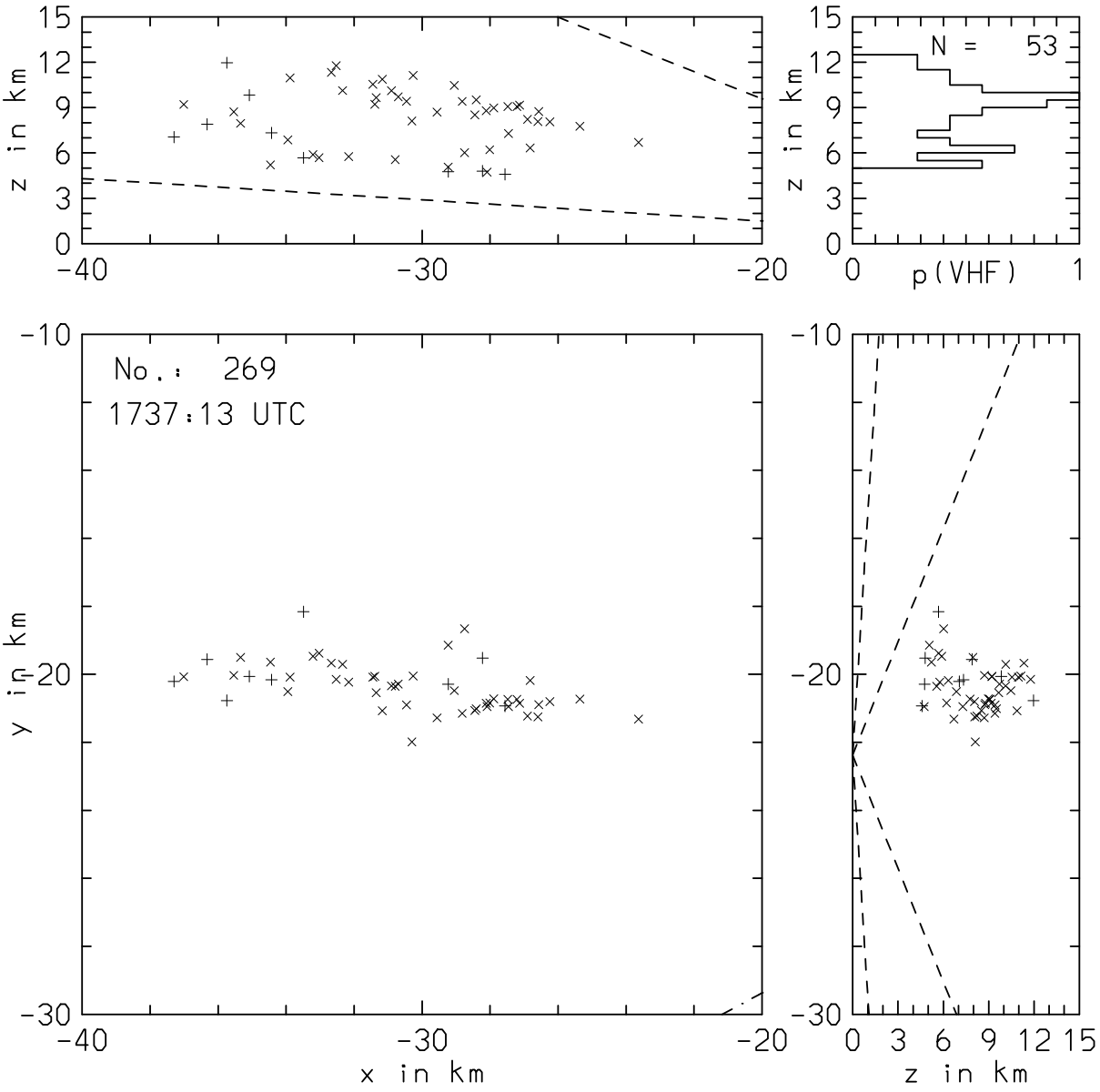
z in km
15
12
9
6
3
0
-40
-30
-20
N = 53
p(VHF)
0
1
No.: 269
1737:13 UTC
y in km
-10
-20
-30
x in km
0 3 6 9 12 15
z in km

Figure 5

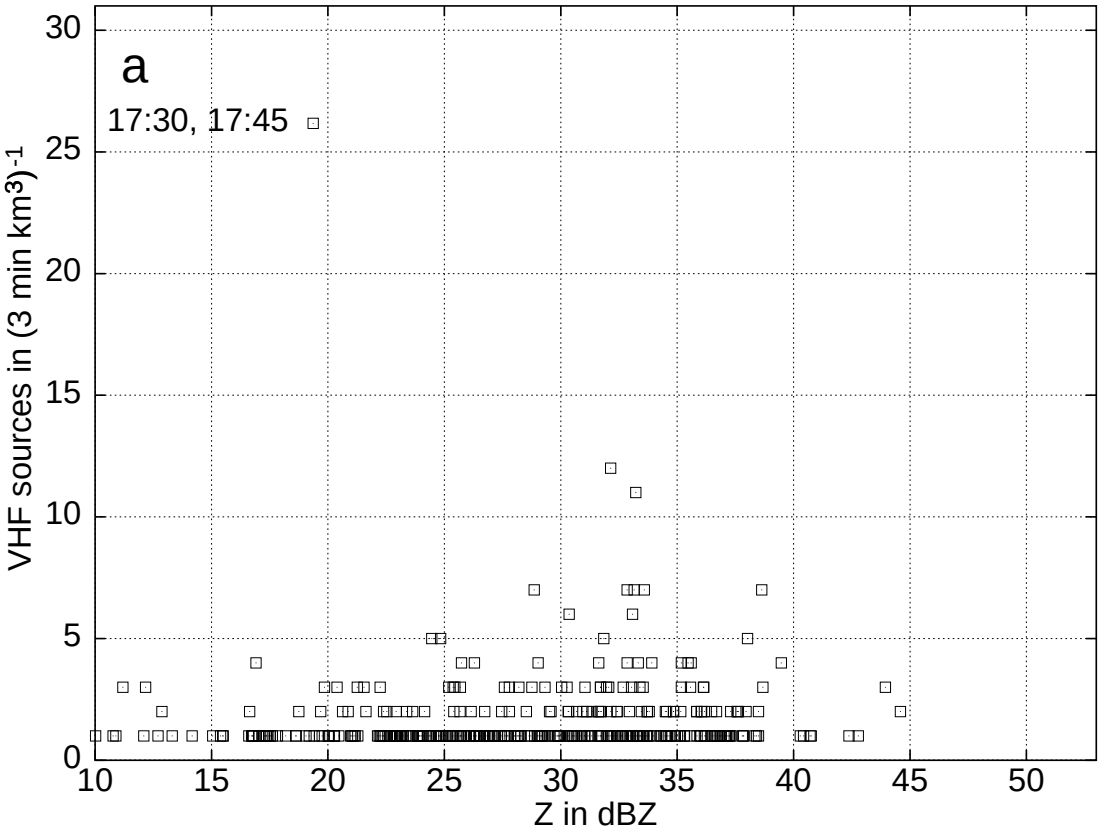
a
17:30, 17:45
VHF sources in (3 min km³)⁻¹
Z in dBZ
0
5
10
15
20
25
30
10
15
20
25
30
35
40
45
50

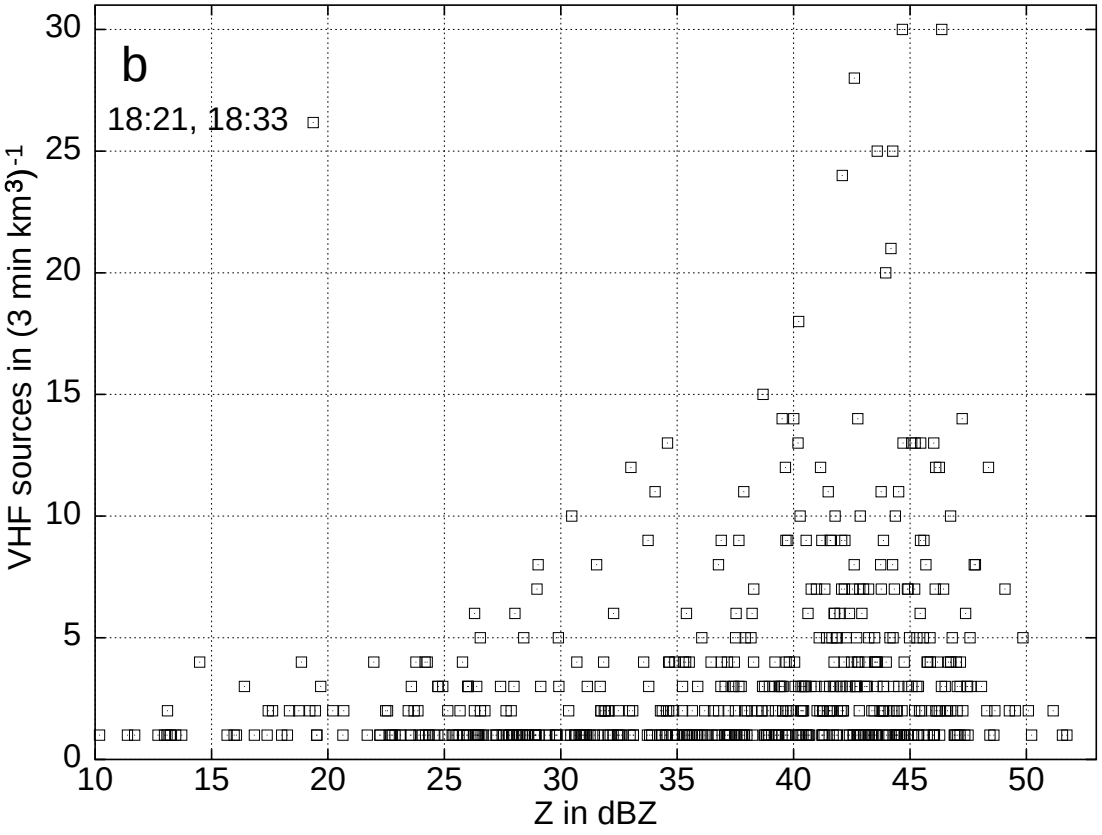
b
18:21, 18:33
VHF sources in (3 min km³)⁻¹
Z in dBZ
0
5
10
15
20
25
30
10
15
20
25
30
35
40
45
50

Figure 6

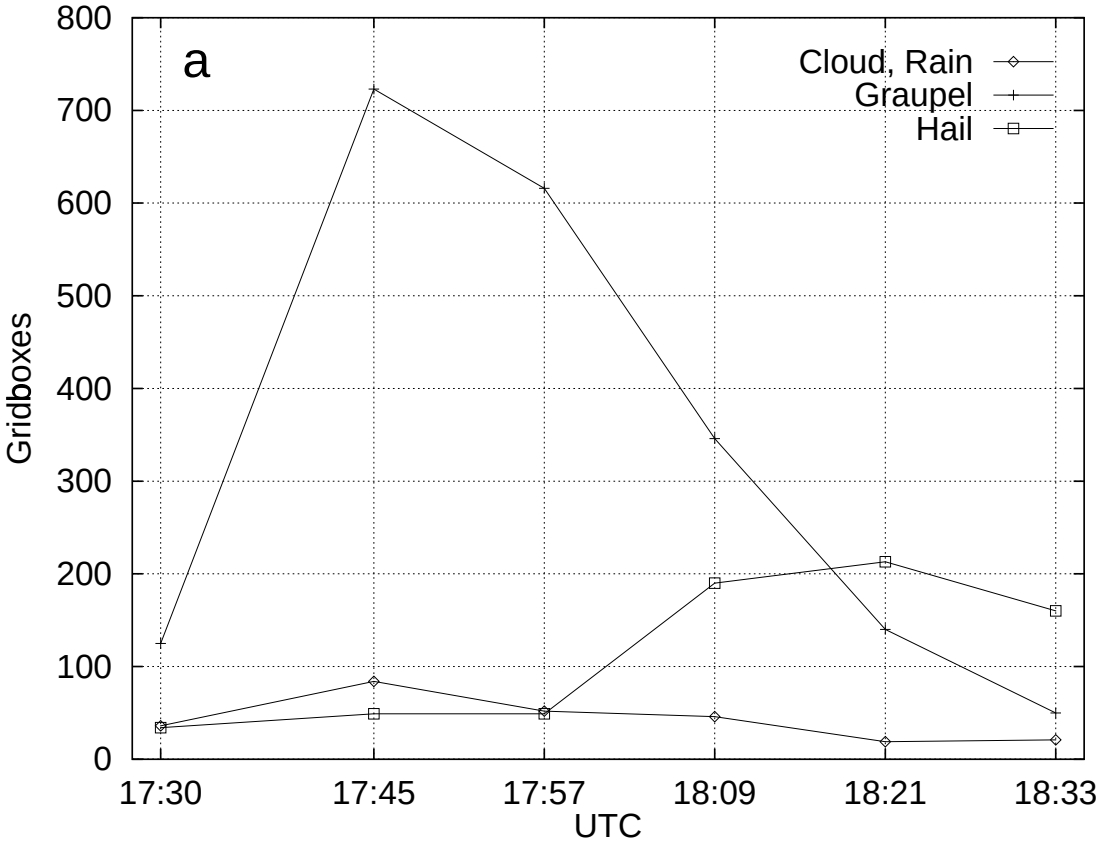
a
Cloud, Rain
Graupel
Hail
Gridboxes
800
700
600
500
400
300
200
100
0
17:30
17:45
17:57
18:09
18:21
18:33
UTC

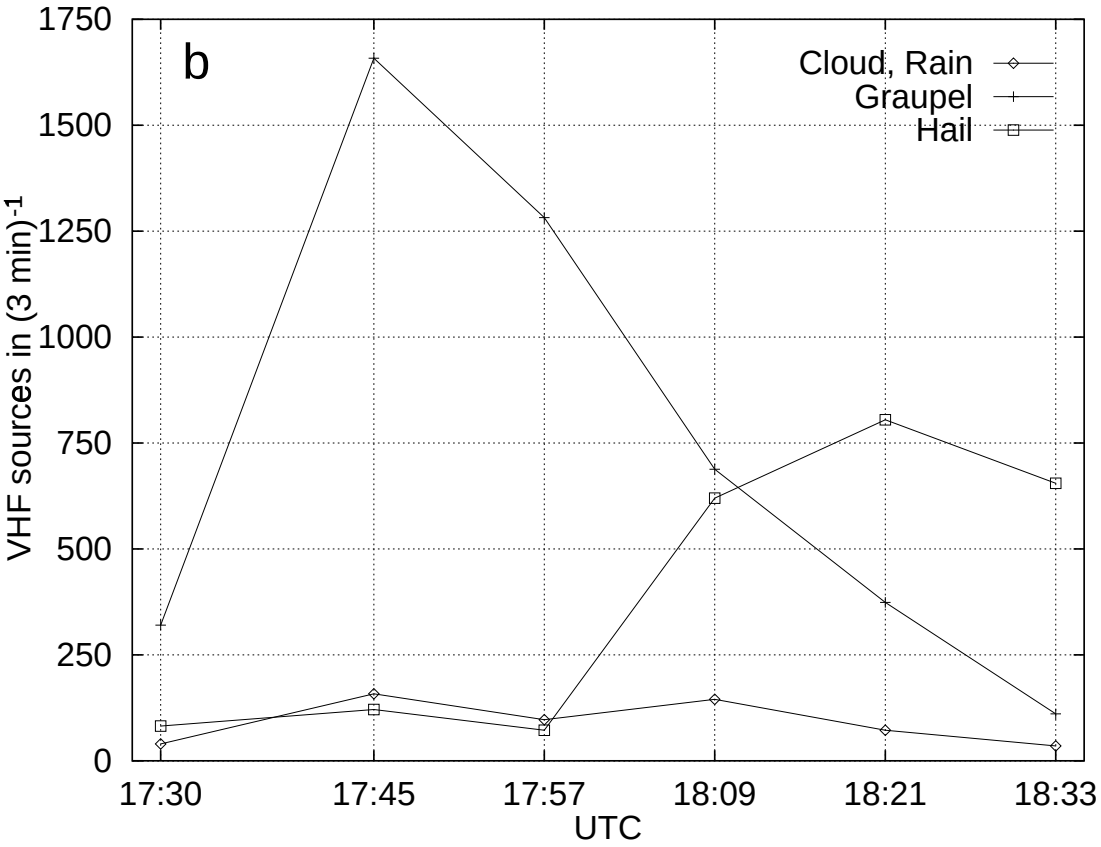
b
Cloud, Rain
Graupel
Hail
VHF sources in (3 min)-1
1750
1500
1250
1000
750
500
250
0
17:30
17:45
17:57
18:09
18:21
18:33
UTC

Figure 7

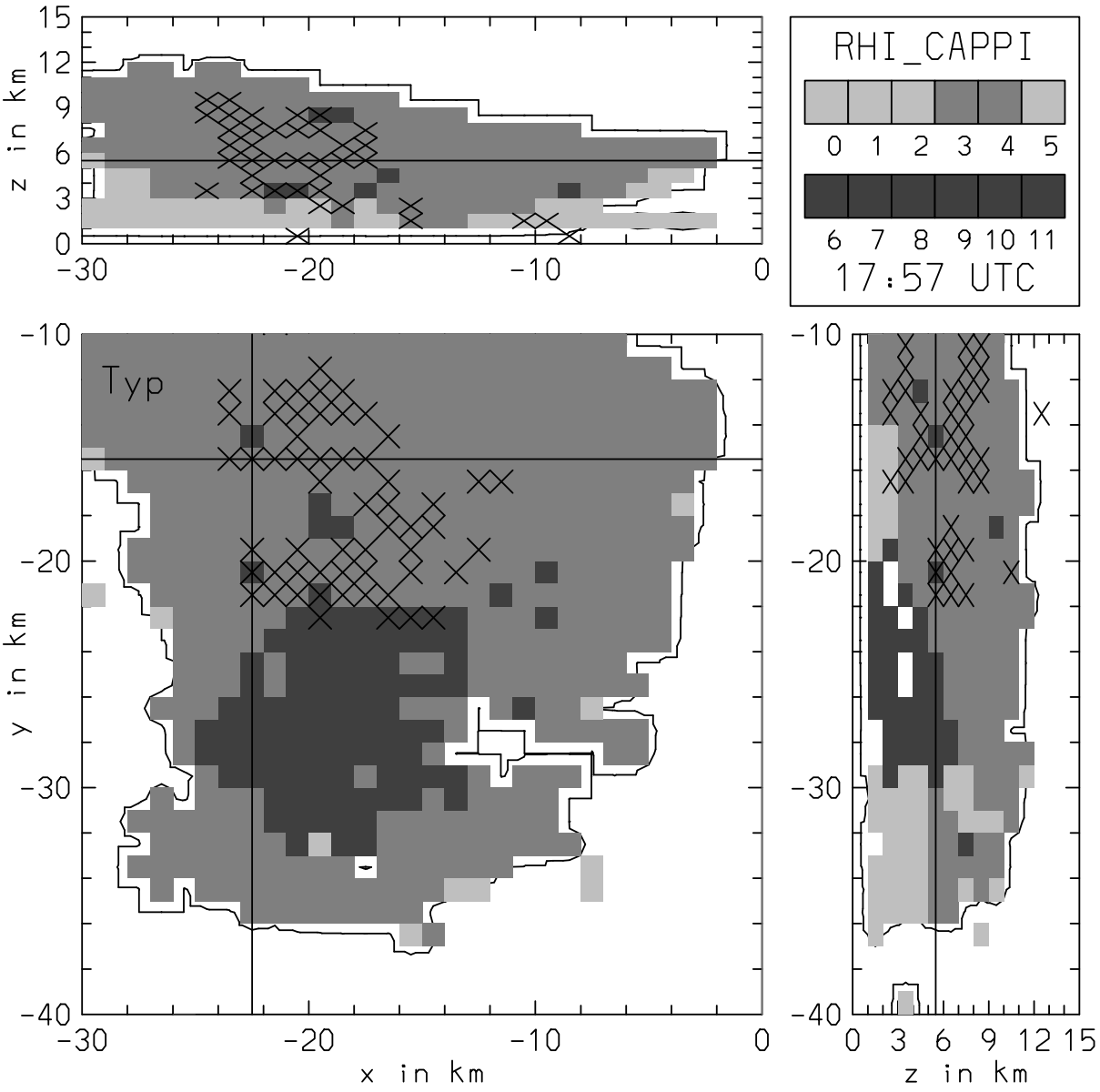
RHI_CAPPI
0 1 2 3 4 5
6 7 8 9 10 11
17:57 UTC
z in km
15
12
9
6
3
0
-30
-20
-10
0
Typ
y in km
-10
-20
-30
-40
x in km
X
z in km
0 3 6 9 12 15

Figure 8

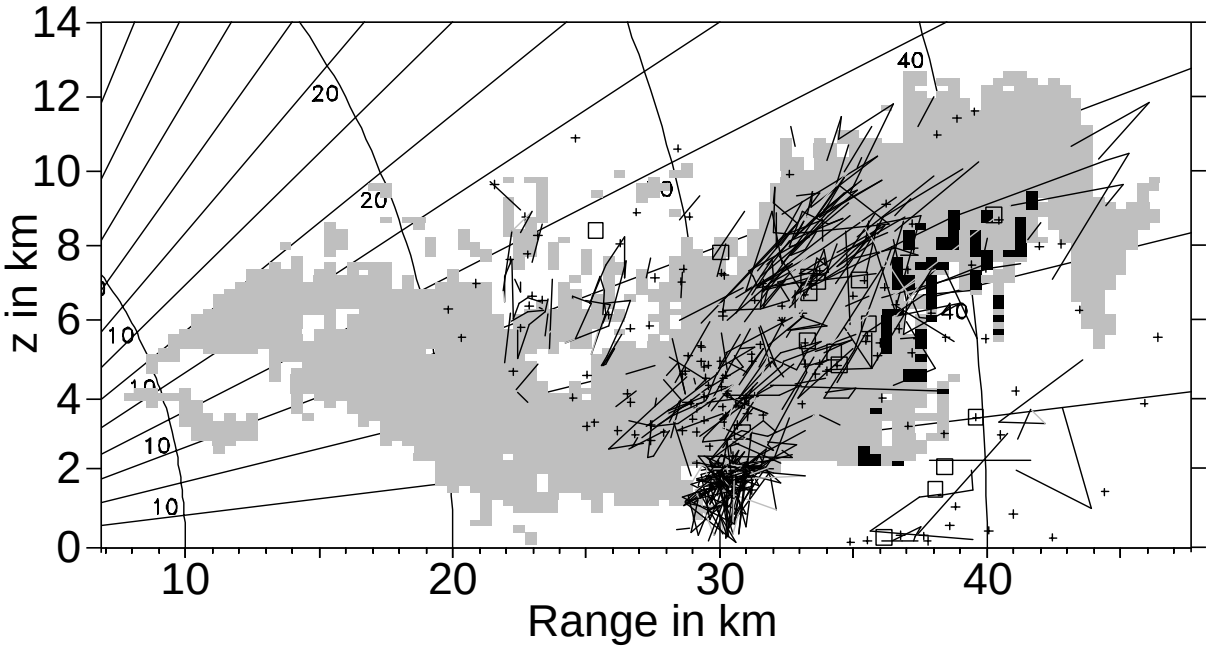

Figure 9